Zeitschrift: Schweizerische mineralogische und petrographische Mitteilungen = Bulletin suisse de minéralogie et pétrographie

Band: 74 (1994)

Heft: 3

Artikel: A 3D crustal model of the Eastern External Aar Massif interpreted from a network of deep seismic profiles

Autor: Hitz, L. / Pfiffner, O.A.

DOI: https://doi.org/10.5169/seals-56356

SCHWEIZ. MINERAL. PETROGR. MITT. 74, 405–420, 1994

A 3D crustal model of the Eastern External Aar Massif interpreted from a network of deep seismic profiles

by *L. Hitz*[1] and *O.A. Pfiffner*[*1]

Abstract

Deep seismic reflection profiling at the transition between Central and Eastern Alps has provided a detailed image of the crustal structure. As part of the Swiss National Science project NFP20, a series of reflection profiles was recorded along strike and dip of the Alpine structural trend. The reflection data were two-dimensionally interpreted. Based on the two-dimensional interpretations, structure contour maps of the base of the European crust, the top of the laminated lower crust, the top of the lower crust and of the basement-cover contact were constructed. The results show that the three lower crustal discontinuities all have similar and simple three-dimensional geometries with general ENE strikes and SSE dips ranging from 8° to 12°. In contrast to the lower crustal discontinuities, the basement-cover contact reveals a highly structured three-dimensional geometry dominated by thrust-tectonics. The structural disharmony with respect to the lower crust implies a crustal decoupling mechanism during the formation of the external Aar massif basement uplift. Comparison of the top-basement topography with mapped surface geology clearly proves a kinematic relation between the eastern Aar massif culmination and the shape of the Prättigau Halfwindow.

Keywords: Alpine tectonics, external massifs, deep seismic profiling, crustal structure, European Geotraverse.

Introduction

The Alpine mountain chain represents the result of a polyphase deformation history associated with the collision of a part of the African plate, the Adriatic promontory, with the European plate. The nearly 1000 km long orogenic belt stretches from the Ligurian Sea to eastern Austria and is subdivided into three main branches: the Western, Central and Eastern Alps. The area of interest to this study is located at the transition between the Central and Eastern Alps (cf. TRÜMPY, 1992). Figure 1 shows the main tectonic units involved. They are from N to S and structurally upward: (1) the Helvetic zone with the allochthonous Helvetic nappes, the parautochthonous cover (= Infrahelvetic) and its crystalline substratum outcropping in the Vättis inlier, (2) the Penninic zone including Bündnerschiefer and Flysch sediments with intercalated ophiolitic material, Penninic basement nappes and Briançonnais cover nappes, (3) the Arosa mélange zone representing the suture between the Penninic and the overlying Austroalpine zone, and (4) the Austroalpine zone consisting of extensive crystalline basement nappes and their sedimentary cover. Unit (1) forms the external zone of the Alps whereas units (2) and (3) form the internal part. Unit (4) represents the overlying orogenic lid (cf. LAUBSCHER, 1983).

Until recently, most of the information about the area concerned (Fig. 1) has been based on outcrop observations over the last roughly 150 years. To enhance the knowledge of the subsurface, the Swiss National Science Foundation program NFP20 (cf. FREI et al., 1989) acquired in 1986 a near-vertical seismic reflection line crossing the study area in a N–S direction more or less perpendicular to the Alpine surface strike. The line was termed E1 or NFP20-Eastern Traverse and formed a contribution to the European Geotraverse (EGT) project. Recording of E1 was accompanied by areal shooting in the E1-receiver spread resulting in three N–S running fan-profiles termed E7, E8 and E9. In addition,

[1] Geologisches Institut, Universität Bern, Baltzerstrasse 1, CH-3012 Bern, Switzerland.
* Corresponding author.

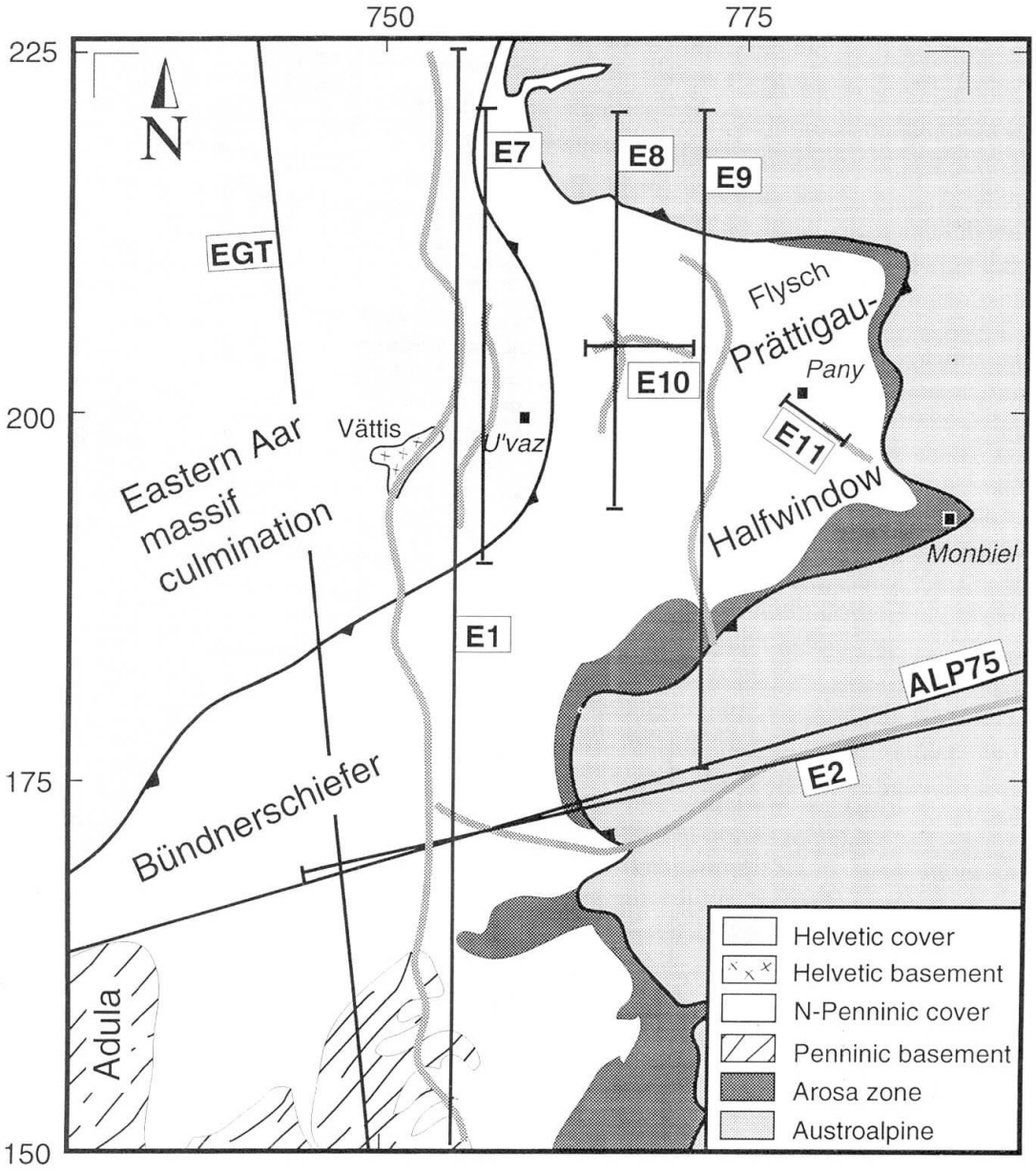

Fig. 1 Simplified tectonic map of the study area with locations of the four deep-seismic profiles E1, E2, E10 and E11, the three fan profiles E7, E8 and E9, and the EGT (YE, 1992) and ALP75 (YAN and MECHIE, 1989) seismic refraction profiles. Grey lines correspond to CMP positions, straight black lines to the traces of the geological cross-sections of figure 5. Squares indicate fan-shot locations and rectangles show the locations of the contour maps of figure 6. Coordinates are given in the Swiss National km-Grid.

two short near-vertical lines, E10 and E11, were shot between lines E8 and E9 and east of line E9, respectively. Finally as one of the last profiles in the NFP20 project, the reflection seismic strike-line E2, which crosses E1 in the west, was registered in 1990. Altogether, the reflection profiles, supplemented by the EGT and ALP75 refraction profiles, form a large-spaced grid of two-dimensional (2D) seismic coverage across the study area (Fig. 1).

The primary focus of this research represents the 2D interpretation of this seismic database with the objective of constructing a three-dimensional (3D) crustal model consisting of four layers: (1) the basement-cover contact, (2) the top of the lower crust (Conrad-discontinuity), (3) the top of the laminated lower crust, and (4) the base of the crust (Moho-discontinuity). This 3D model forms the base of the evaluation of large-scale tectonic features at the transition of Central and Eastern Alps and – in a N–S direction – of external and internal Alps. Special attention is thereby given to the eastern continuation of the external Aar massif basement uplift.

Seismic data

In the following, each 2D seismic reflection profile is briefly presented (Figs 2a to 2g). They are shown unmigrated in an apparent line drawing format. The line drawing appearance was achieved by plotting only the strongest positive amplitudes following coherency filtering. Reflections of interest are labelled with letters and are discussed in the following section.

Figure 2a shows the results of line E1 excluding the southernmost part. The first 8 s represent Vibroseis recordings whereas from 8 to 20 s, dynamite data are shown. The full-length Vibroseis as well as the corresponding dynamite section are presented among others in VALASEK et al. (1991) or PFIFFNER et al. (1990b), where also details on recording, data processing and geologic interpretation are given. In the here presented extract of line E1, upper crustal reflections down to around 5 s are prominent in the N and in the S, with the central part being largely seismically transparent. At mid-crustal levels no clearly coherent reflections can be observed. Between 9 and 15 s an upper weakly defined reflection band and a lower approximately 1 to 1.5 s thick reflection band both S-dipping can be traced across the northern half of the profile.

Figures 2b to 2d represent the fan profiles E7 to E9. Details on recording and processing parameters of these profiles as well as detailed geologic interpretations can be found in HITZ and PFIFFNER (1995c). Line E7 (Fig. 2b) has an average lateral offset of 5.4 km only. It is characterized by an approximately 1.5 s thick reflection package with its base dipping from 13.5 s in the N to 14.2 s in the S. In addition, a weakly defined subhorizontal reflection band can be seen between 9.5 and 10 s. It is included in the geologic interpretation, as it can be correlated with coherent reflections in similar position and with similar dip in neighboring profiles. The seismically transparent upper crust corresponds to the transparent central part of line E1 (Fig. 2a).

Fan line E8 (Fig. 2c) has an average lateral offset of 23.0 km. It shows a well developed deep reflection package with its base dipping southward from 13.9 to 14.2 s. Its thickness is in the order of 1.5 s. N-dipping reflections between 11 and 10 s and S-dipping reflections between 9 and 10 s are also present. Reflected energy at 7.5 s in the center of E8 will not be considered for interpretation due to the lack of equivalent, clearly coherent reflections in the neighboring profiles E1, E7 and E9.

The eastern most fan profile E9 (Fig. 2d) has an average lateral offset of 40.0 km and hence the seismic data begin at around 4 s only. It essentially reveals the same deep reflectivity as the previous two profiles, i.e., a S-dipping reflection package from 14 to 15.7 s with a thickness in the order of 1.5 to 2 s, and a less coherent S-dipping reflection band from 10 to 12 s. Despite their small lateral extension, S-dipping reflections at 4 to 6 s between horizontal km 20 and 27 and N-dipping reflections at around 6 s between horizontal km 30 and 34 should be noted. As will be shown below, they can be correlated with reflections in lines E2 and E10.

Figure 2e represents the western part of the WSW–ENE running E2 strike-line. The full-length line as well as details on recording, processing and interpretation can be found in HITZ and PFIFFNER (1995a). Line E2 shows a considerably lower data quality as compared to for example line E1. This observation is explained by the single-fold coverage of the E2-explosion data and by the interference of focussed out-of-plane reflections in the strike-line (cf. HITZ and PFIFFNER, 1995a). The upper crust imaged in E2 is characterized by several, strongly discontinuous reflection groups down to about 8 s. They are all dipping to the ENE. From 8 to about 14 s correlatable coherent reflectivity is absent. It resumes between 14 and 17 s with an approximately 1.5 s thick reflection band dipping shallowly to the ENE.

Line E10 (Fig. 2f), located between the fan profiles E7 and E8 (Fig. 1), represents a near-vertical dynamite data-set. Due to the very low source energy (1.2 kg), only reflections from the upper crust were recorded. The line shows two distinct apparently east-dipping reflection groups at 1.2 in the W to 1.6 s in the E and at 1.8 to 2.3 s, respectively. At the western end of the profile, the lower reflection band flattens out, whereas the upper band looses its strong reflectivity almost completely. Sporadic reflections below the lower reflection band are considered as random noise from a nearby timber factory.

Line E11 (Fig. 2g), representing again a low-energy near-vertical profile, reveals a strong SE-dipping reflection band from 2.7 s in the NW to 3.2 s in the SE and a discontinuous band from 3 s in the NW to approximately 3.5 s in the SE, i.e. similar to the reflection bands in line E10. Above the latter two, an almost 1 s thick subhorizontal to slightly NW-dipping reflective zone between 1 and 2 s can be observed. This zone as well as the upper reflection bands of lines E10 and E11 are not included in the geologic interpretation of this study as - as will be seen later - they stem from above the basement-cover contact.

The results of the EGT and ALP75 refraction

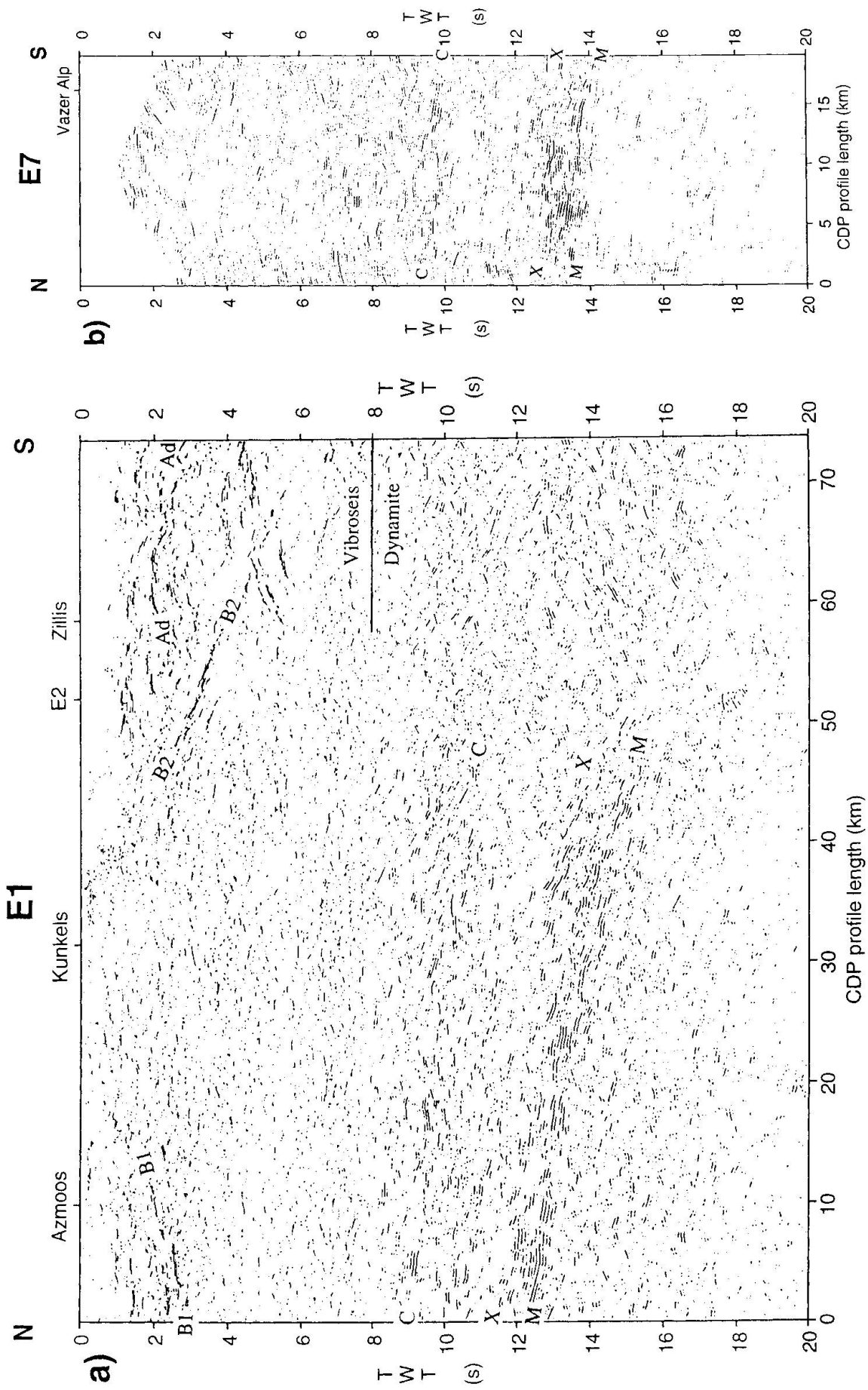
a)
N
S
E1
Azmoos
Kunkels
E2
Zillis
Ad
B2
B1
Vibroseis
Dynamite
C
X
M
T W T
(s)
CDP profile length (km)
b)
N
S
E7
Vazer Alp
CDP profile length (km)

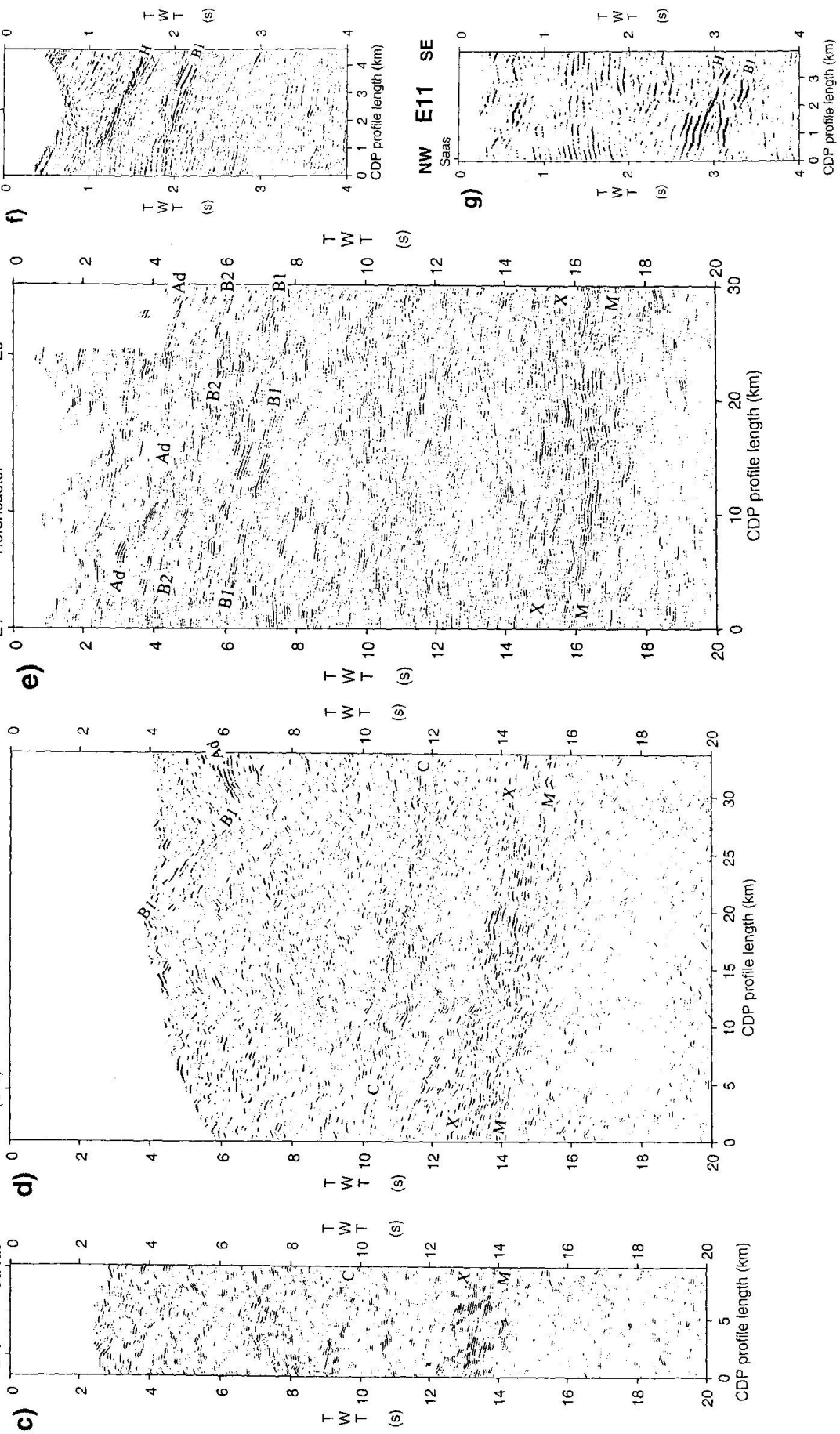

Fig. 2 Unmigrated deep-seismic reflection profiles shown as apparent line drawings. With the exception of line E1, dynamite was used as source-energy. The sections are plotted 1:1 at an average crustal velocity of 6.0 km/s (1 s ≈ 3 km). a) Central part of the near-vertical line E1 taken from VALASEK (1992). The full-length line is presented in VALASEK (1992) and PFIFFNER et al. (1990b). Vibroseis data are shown from 0 to 8 s, dynamite data from 8 to 20 s. b) Fan-line E7. Fan-shot location is Untervaz (see Fig. 1). c) Fan-line E8. Fan-shot location is Pany (see Fig. 1). d) Fan-line E9. Fan-shot location is Monbiel (see Fig. 1). e) Western part of the near-vertical strike-line E2. The full-length line is presented in HITZ and PFIFFNER (1995a). f) Near-vertical line E10. g) Near-vertical line E11.

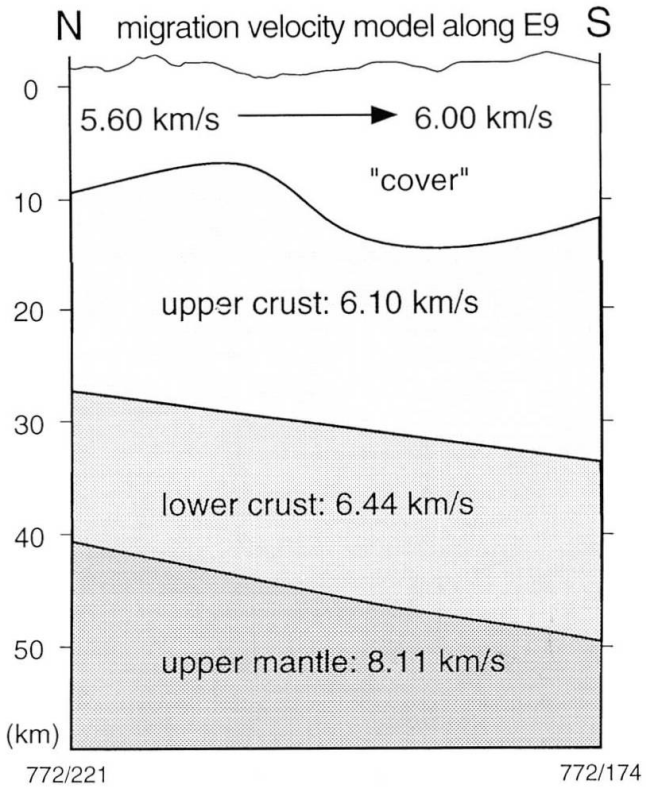

Fig. 3 Example of a simplified three-layer velocity model used for depth-migrating the seismic reflection data presented in figure 2. The model follows line E9 and was obtained by smoothing the detailed velocity structures of a network of Alpine refraction profiles (EGLOFF, 1979; YAN and MECHIE, 1989; YE, 1992). Migration-velocities for mantle, lower crust and upper crust are constant for all lines. Migration-velocities for the "cover" vary laterally from 5.6 km/s in the N to 6.0 km/s in the S. H : V = 1 : 1.

data (Fig. 1) are presented in YE (1992) and YAN and MECHIE (1989), respectively. For this study, the structures of interest are the refraction-derived Moho discontinuity separating the lower crust from the mantle, and the top of the lower crust, the so-called Conrad discontinuity separating upper from lower crust. In addition, the velocity structures served as the basis for a simplified velocity model used for depth-migration of the reflection seismic data (Fig. 3).

2D geologic interpretation

For the purpose of the 2D geologic interpretation, a computer-based transformation of the reflection seismic data into line drawings using a program developed by VALASEK (1992) followed by ray-theoretical depth migration (cf. HOLLIGER and KISSLING, 1991) were performed. The 2D velocity models used for depth migration were determined by associating smoothed 1D velocity functions obtained from a network of Alpine refraction profiles (EGLOFF, 1979; YAN and MECHIE, 1989; YE, 1992) to the unmigrated reflection boundaries described above and then converting the resulting time structure to depth (Fig. 3). After migration the above described reflections were identified in the depth-migrated sections. The results of this processing are shown in the simplified line drawing of figure 4. The unmigrated profile length is represented by a grey bar at the bottom of each section. Note that up-dip migration of reflections, especially in the case of lines E7 through E9 (Figs 4b to 4d) considerably increases the profile lengths. The length of the geologic profiles presented in figure 5 is thus determined by the length of the migrated sections (Fig. 4).

For the geologic interpretation the following information was used: (1) depth-migrated reflection geometry (Fig. 4), (2) refraction-derived velocity-depth models (EGLOFF, 1979; YAN and MECHIE, 1989; YE, 1992), (3) surface geology (cf. LORENZ, 1901; BRAUCHLI and LEUPOLD, 1915; TRÜMPY, 1916; CADISCH, 1922; BRAUCHLI and GLASER, 1924; EUGSTER and LEUPOLD, 1930; NABHOLZ, 1945; NÄNNY, 1948; CHRIST and NABHOLZ, 1959; TOLLMANN, 1976; OBERHAUSER, 1980; TRÜMPY, 1980; ALLEMANN et al., 1985), and (4) interpretations of intersecting or neighboring reflection profiles. This information generally allows the identification of the migrated reflections presented in figure 4. In the following, interpretation results are given starting with the deepest reflections and proceeding upwards to the basement-cover contact. The interpretations are summarized in the geologic cross sections of figure 5.

The base of the reflective zone between *X* and *M* (Figs 4a to 4e) is interpreted as the base of the crust, i.e., the Moho discontinuity (Figs 5a to 5e). This interpretation is based on depth position and dip of *M*, which can be correlated with a p-wave velocity jump from 6.5 km/s to 8.3 km/s in the EGT seismic refraction profile (YE, 1992) and with a velocity jump from 6.35 km/s to 8.1 km/s in the ALP75 seismic refraction profile (YAN and MECHIE, 1989). In addition, the strong reflectivity between *X* and *M* is characteristic for the lower crust immediately above the Moho in the external Alps (cf. VALASEK, 1992) and in many sampled areas in Phanerozoic Europe (cf. DEKORP, 1990) and the basin-and-range province (cf. KLEMPERER et al., 1986). The southward dip of the Moho in the N–S sections ranges from 9° in line E7 to 12° in the line E1 (Figs 4a to 4d), with dip-variations illustrating rather the uncertainity in dip-determination than a true dip gradient. In the

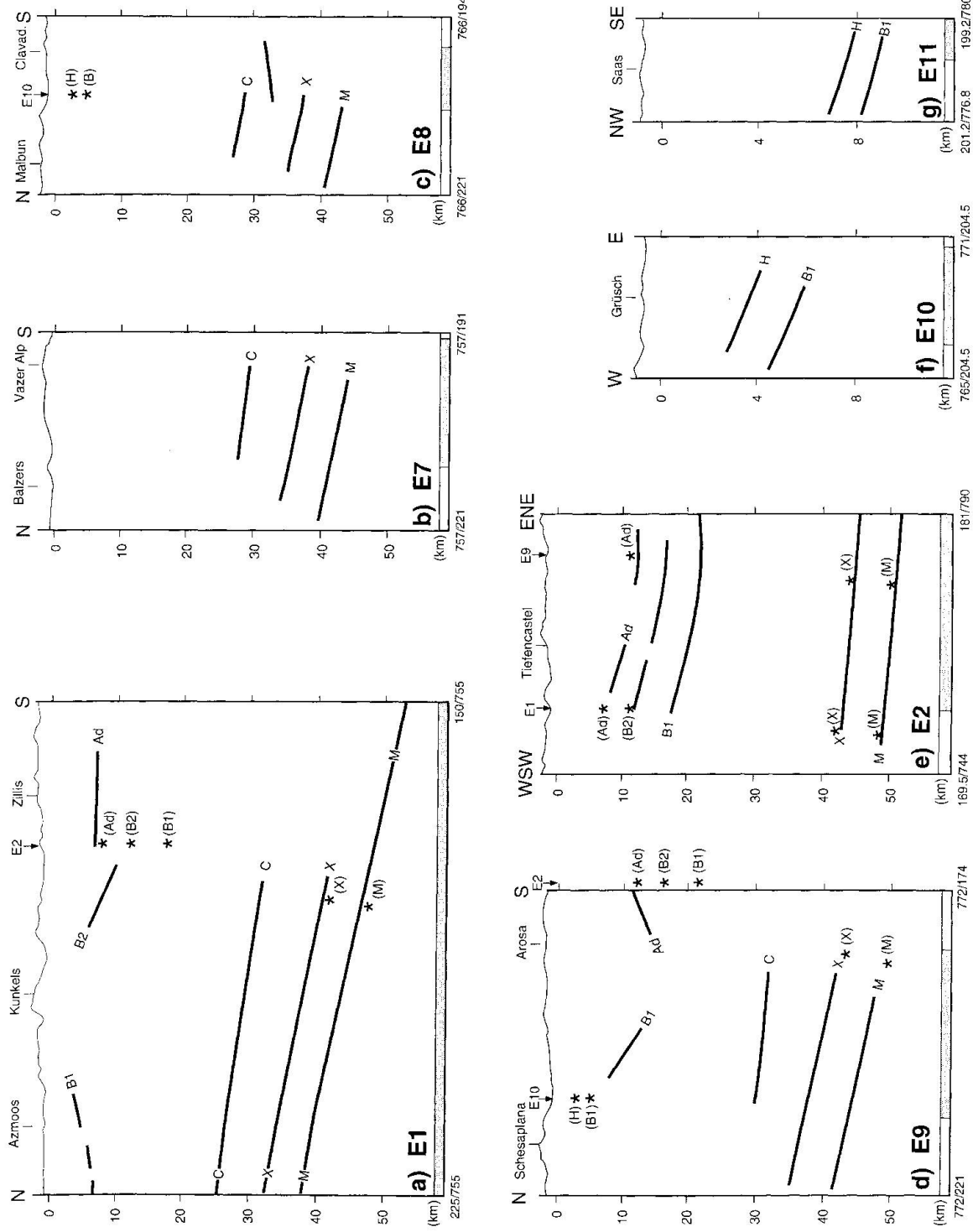

Fig. 4a–g Depth-migrated reflections considered for interpretation of the seismic data presented in figure 2. White bars at the bottom of each section correspond to the profile length added by the migration process (up-dip migration of dipping reflections). Stars correspond to migrated reflections of intersecting profiles (partly linearly extrapolated) with lower crustal reflections laterally hand-migrated. Coordinates are given in the Swiss National km-Grid. H : V = 1 : 1. M: Moho, X: top of laminated lower crust, C: Conrad, B1: top of Aar massif basement, B2: top of Gotthard "massif" basement, H: top of Infrahelvetic cover, Ad: top of Adula basement nappe.

strike-line E2 (Fig. 4e), the Moho dips more gently with about 3° to the east indicating a general ENE strike of this discontinuity in the area sampled.

The highly reflective zones immediately above the Moho (between *M* and *X* in Figs 4a to 4e) are interpreted as the seismic expression of a laminated lower crust with *X* representing its top (Figs 5a to 5e). Such heterogeneous reflection fabrics have been reproduced by synthetic modeling of a 2D stochastic model of the Strona-Ceneri/Ivrea zones by HOLLIGER and LEVANDER (1994). The authors conclude from their work that the lower crustal reflectivity is predominantly depending on the lithological population present, i.e. a subhorizontal layering between high and low-velocity lithologies like silicic and mafic, mafic and ultramafic, or silicic and ultramafic rocks, contacts which all provide the required impedance contrasts (KERN and RICHTER, 1981). The lithologic layering may have originated from stretching of a thickened and thermally relaxed heterogeneous lower crust during post-thickening crustal collapse. In the case of the Alpine laminated lower crust, REY (1993) suggests a Late-Variscan age for this event. The thickness of the laminated lower crust in the seismic lines is in the range of 4 to 5 km and compares with the one in the Western Alps (cf. VALASEK, 1992) or the Pyrenees (cf. BOIS and ECORS, 1991). Dip and orientation of the top of the laminated lower crust are virtually identical with the ones determined for the Moho discontinuity. The lack of lower crustal reflectivity towards the S in line E1 (Figs 2a and 4a) is discussed in the following section.

The erratic line-up of short reflections labelled *C*, which is present in all deep sections in a depth range of 25 to 34 km excluding line E2 (Figs 4a to 4d) is interpreted as marking the top of the lower crust, i.e., the Conrad discontinuity (Figs 5a to 5d). This interpretation is based on the correlation with a p-wave velocity jump from 6.2 km/s to 6.5 km/s with similar depth position and dip in the EGT refraction profile (YE, 1992). The southward dip of this discontinuity in the N–S sections is generally smaller than the Moho dip with 7° in lines E1, E7 and E9, and 10° in line E8 and is indicative of a minor southward thickening of the lower crust at least along line E1. In the strike-line E2 (Fig. 2d) and in the southernmost part of E1 (Fig. 2a), the top of the lower crust is not defined. Again, this lack is discussed in the following section.

Reflection *B1* which is also present in the low-energy near-vertical profiles E10 and E11 (Figs 4f and 4g) is interpreted as stemming from near the top of the external Aar massif (Fig. 5). This interpretation is partly based on surface correlation (PFIFFNER et al., 1990b, constrained by 3D-modelling by STÄUBLE et al., 1993) and partly on the observation that *B1* marks the last coherent reflections above the Conrad reflections, i.e., the external basement lacks the required lithological population or geometry to produce reflections. The external Aar massif is thus seismically transparent (cf. PFIFFNER et al., 1990b). Reflectivity of *B1* presumably does not stem from the basement-cover contact itself but from a high-velocity dolomite layer immediately above the basement-cover contact (cf. SPRECHER and MÜLLER, 1986; LEVATO et al., 1994). *B1* in line E10 (Fig. 2f) can be seen to flatten out and to loose reflectivity towards the west. This suggests that the basement-cover contact might change its orientation from an apparent E-dip to a more horizontal orientation. In this case, coherent seismic energy would reflect out of the E10 receiver spread and thus would explain the loss of coherent reflections towards the west. The implied westward flattening could further indicate, that the crest of the ENE-dipping Aar massif culmination is situated immediately to the west of the migrated E10-section. Assuming that this interpretation is correct, joining of the postulated Aar crest with the Aar crest exposed at surface in the Vättis inlier (Fig. 1) results in an orientation of the Aar massif's crest-line of approximately N60°E with a dip of 20°. This orientation agrees well with the surface orientation of major fold axes in the crystalline basement, which were formed during the basement uplift (PFIFFNER, 1977). *B1* is also recorded in line E9 (Fig. 4d) where it can easily be correlated with the basement top recorded in line E10. *B1* in line E2 finally has no seismic equivalent in the intersecting line E1 (Fig. 1). The lack of correlation is attributed to difference in structural style as the basal Helvetic thrust in line E1 is located at the base of the Permian "Verrucano" clastics and thus the contact between the Helvetic substratum (Aar massif) and the overlying S-Helvetic Gotthard thrust-sheet puts basement rocks onto basement rocks, a configuration apparently lacking the appropriate impedance contrast to produce strong reflections. Towards the E of line E1, i.e., in the area of line E2, the basal Helvetic thrust ramps laterally up into middle Jurassic shales (TRÜMPY, 1969; PFIFFNER, 1993). Therefore, in the area of line E2, Triassic to lower Jurassic sediments presumably remained attached to the Aar massif and were overridden by the Gotthard thrust-sheet. Such lithologic layering can easily explain the comparatively strong reflectivity of the top of the Aar massif in line E2.

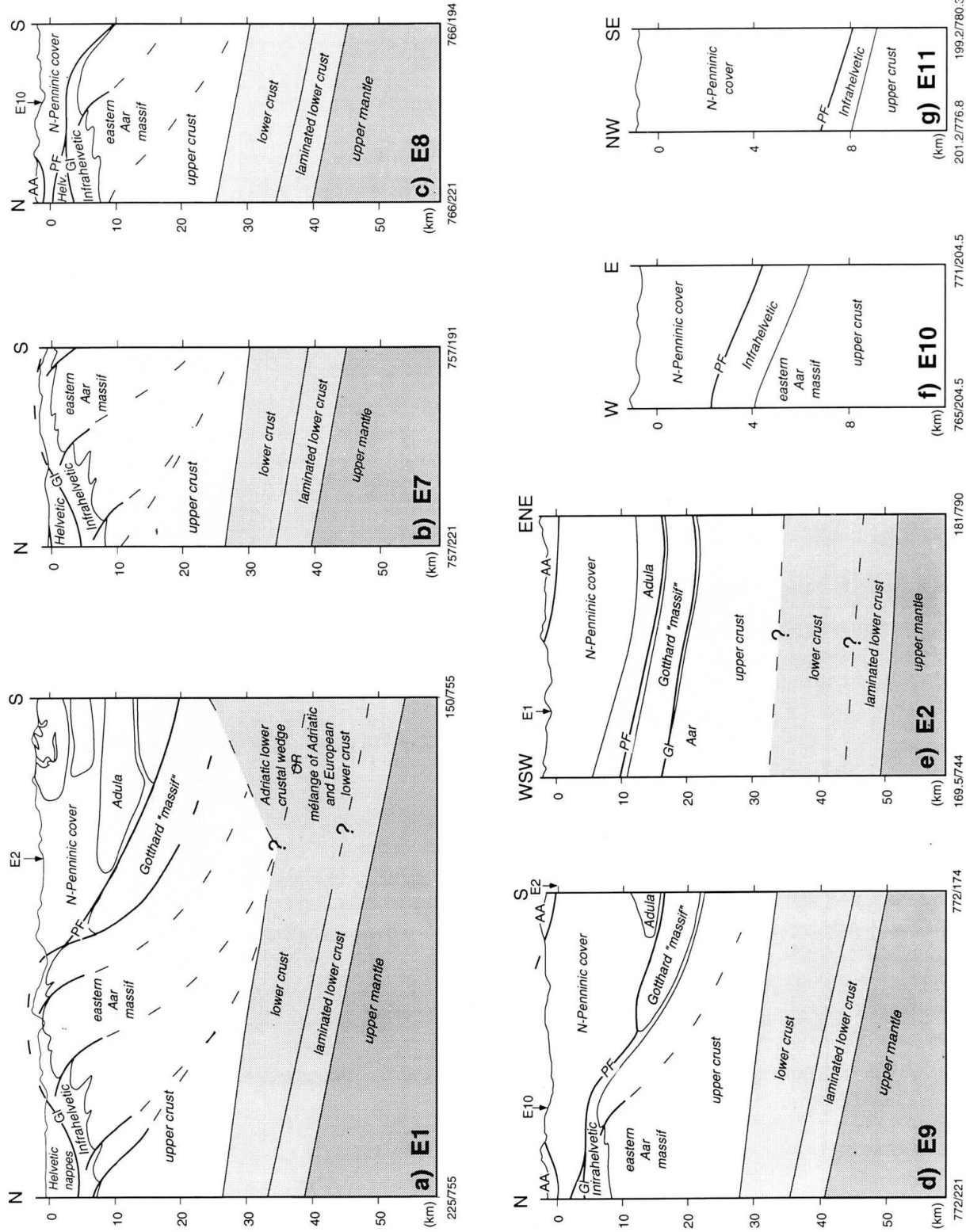

Fig. 5a–g Geologic cross sections along the depth-migrated sections shown in figure 4. Interpretations of the seismic data are based on surface correlation, and on the correlation with intersecting or neighboring reflection and refraction profiles. The traces of the cross sections are straight and are shown as black lines in figure 1. Coordinates are given in the Swiss National km-Grid. H : V = 1 : 1. AA: Austroalpine, Gl: Glarus thrust, PF: Penninic Front.

As recording offsets were generally too large to register the top of the crystalline basement in the fan profiles E7 to E9, the top of the Aar massif must be projected from surface and from subsurface positions recorded in lines E1 and E10. For the Aar massif's crest-line, the orientation of N60°E/20° deduced above was used for projection. As a second key-structure, the deepest basement position north of the culmination, the "Aar depression" trending N65°E (cf. HITZ and PFIFFNER, 1995b), was used. For the further construction of the basement top between projected crest and depression, the two key-structures were joined by a straight line, which served as an envelope for the northern flank of the Aar massif. Its more detailed geometry was then taken from the 2D and 3D-modeled structure of the E1 profile by STÄUBLE and PFIFFNER (1991) and STÄUBLE et al. (1993).

Reflections labelled *B2* are registered in lines E1 and E2 (Figs 4a and 4e). Based on large-distance surface projection and on the postulation that the Gotthard massif represents the substratum of the Helvetic Säntis-Drusberg nappe (PFIFFNER, 1985; WYSS, 1986), *B2* was interpreted as the top of the S-Helvetic Gotthard massif by PFIFFNER et al. (1990b), which at the same time corresponds to the Penninic Front (Figs 5a, 5d, 5e). It has to be stressed, however, that this interpretation is ill-constrained and that *B2* could also represent the top of a basement thrust-sheet associated with the Aar massif uplift, i.e., that the Gotthard massif lacks an eastern continuation. In attendance of better constraints, however, we retain the first interpretation.

The structurally highest upper crustal reflections discussed in this study are the reflections labelled *Ad*. They occur in lines E1, E2 and E9 and correlate well among the three lines (Figs 4a, 4d, 4e). Projections of surface data (PFIFFNER et al., 1990b) over 20 km (!) place the top of the N-Penninic Adula basement nappe at around 7 km depth beneath Zillis in line E1 (Fig. 4a). The reflections *Ad* are thus interpreted as defining this boundary (Figs 5a, 5d, 5e). This interpretation is consistent with the 3D modelling results by LITAK et al. (1993). Reflectivity can be explained with lithological velocity contrasts between high-velocity cover sediments and the Adula crystalline basement rocks.

3D model

The 2D interpretations discussed above and summarized in the geologic cross sections of figure 5, together with the EGT (YE, 1992) and ALP75 (YAN and MECHIE, 1989) refraction profiles form a dense network of 2D crustal information. Based on this network, structure contour maps for the following European crustal discontinuities were constructed: the base of the crust (Moho discontinuity, Fig. 6a), the top of the laminated lower crust (Fig. 6b), the top of the lower crust (Conrad discontinuity, Fig. 6c) and the top of the structurally highest crystalline basement units (Fig. 6d). The 3D geometry of the three lower crustal discontinuities were obtained by linear interpolation between the 2D sections and subsequent smoothing with a 2 km long running average filter (program INTERPS by VALASEK, 1992). Contouring of the top basement surface was entirely made by hand. The accuracy of the vertical position of the different interfaces is difficult to quantify. One important controlling parameter is the velocity function used for depth-migration (cf. HOLLIGER and KISSLING, 1991). In the area studied, the vertical errors for a velocity fluctuation of 0.2 km/s relative to 6.0 km/s are approximately 1.8 km for the Moho discontinuity, 1.2 km for the Conrad discontinuity and 0.5 km for top basement surface. Another source of error are depth distortions induced by out-of-plane reflections. 3D-modelling by VALASEK (1992) and LITAK et al. (1993) suggests that in the N–S profiles errors due to out-of-plane reflected energy are in the order of 0.5 km for the Moho and Conrad discontinuities, and up to 1.5 km for the top of the crystalline basement in the area considered. Finally, additional errors are introduced by the uncertainty in picking the right reflections as the crustal boundaries are very often defined by a line-up of short reflections with varying travel times. For an error of 300 ms at an average velocity of 6.0 km/s, we would have to add 0.9 km to the above vertical errors. Assuming that the overall interpretation is correct we therefore conservatively estimate an average vertical error of ± 3 km for the Moho and the top of the laminated lower crust, and ± 2.5 km for the Conrad discontinuity. The depth accuracy of the top of the crystalline basement might vary as much as ± 3 to 0 km (surface control). Note, however, that for the objective of defining the general relationships between the main crustal boundaries, the errors are insignificant.

Moho discontinuity (Fig. 6a): The contours of the Moho discontinuity are constrained by both reflection and refraction seismic data (grey lines in Fig. 6a). The Moho geometry reveals a smooth surface with an average strike of N70°E and an average dip of 12°. Comparison with the Moho map in this area by VALASEK (1992) shows a remarkably good agreement in strike and dip, with depth positions differing by a maximum of 1 km. The good agreement illustrates the relatively sim-

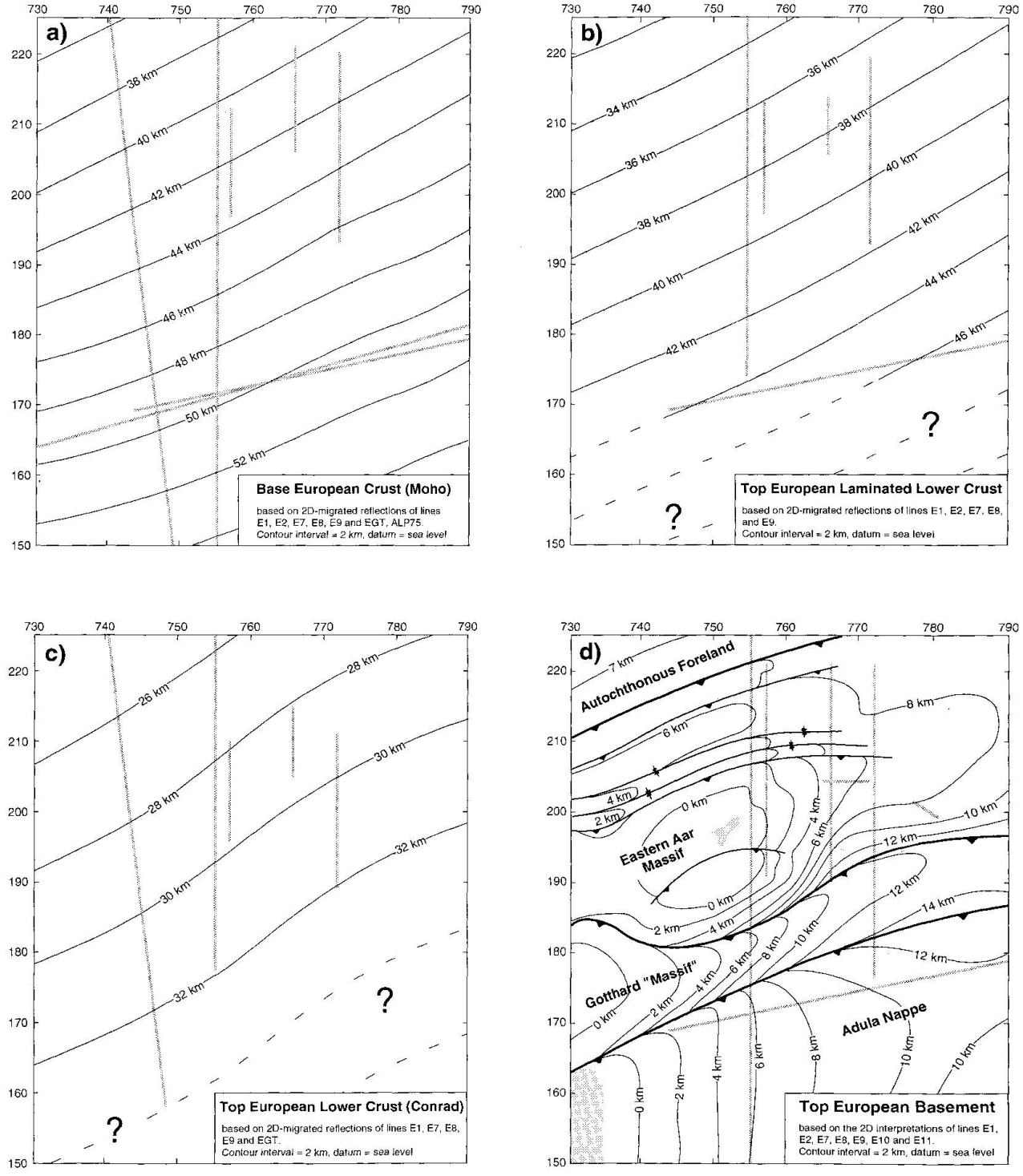

Fig. 6a–d Structure contour maps of the crustal discontinuities imaged in the seismic reflection data of figure 2 and the EGT and ALP75 seismic refraction profiles (grey lines). Lower crustal discontinuities (a, b, c) show similar and simple 3D geometries with a constant ENE strike and dip angles between 12° (Moho and top of the laminated lower crust) and 8° (Conrad). The 3D geometry of the top basement (d) reveals complicated domal surfaces formed by a combination of fold-and-thrust tectonics. The structural disharmony with respect to the lower crust implies a crustal decoupling mechanism during the formation of the external basement uplift (Aar) and nappes (Gotthard, Adula). Coordinates are given in the Swiss National km-Grid.

ple and continuous geometry of the European Moho, considering that Valasek's map is based on a far less dense network of 2D seismic lines. In addition, the good fit between the refraction and the reflection derived Moho illustrates that the two methods are imaging the same discontinuity.

Top of laminated lower crust (Fig. 6b): The top of the laminated lower crust is constrained by the migrated reflections only (grey lines in Fig. 6b). As might be expected from the 2D data, the 3D geometry of the top of the laminated lower crust is nearly identical with the Moho geometry. The two discontinuities are separated by 4 to 5 km. This thickness compares to the ones determined in the central and western portions of the Swiss Alps (cf. VALASEK, 1992). However, it is only half the thickness of the laminated lower crust found in DEKORP profiles in the European foreland (cf. DEKORP, 1990). Assuming a pre-Alpine origin of this structure (REY, 1993), it is possible that the reduced thickness resulted from crustal thinning and stretching during Mesozoic rifting. Another point of interest regarding the laminated lower crust is the fact that south of approximately km 170 of the Swiss National grid system, the laminated lower crust looses its characteristic strong reflectivity almost completely (stippled contours in Fig. 6b). At surface this zone corresponds roughly to the transition between external and internal Alps. In the subsurface, the transition from a reflective to a non-reflective laminated lower crust coincides – depending on the tectonic model – either with the northern tip of a lower crustal Adriatic indenter (Fig. 5a, PFIFFNER et al., 1990b), or with the northern boundary of a mélange zone consisting of European and Adriatic lower crust (LAUBSCHER, 1994). These observations lead us to the postulation that the lack of a reflective lower crust is related to the difference in crustal deformation between the external and internal Alpine domains, i.e., strong energy scattering due to nappe stacking and due to lower crustal deformation in the internal domain versus comparatively unscattered seismic energy in the external basement uplift and in the undeformed lower crust in the external domain. Whether the scattering of the seismic energy takes place in the deformed lower crust itself or in the structurally complex overburden is a matter of debate (cf. PFIFFNER et al., 1990b; HOLLIGER and KISSLING, 1991). If the first possibility is true, the lack of a reflective lower crust could be indirectly used to map the northern extent of deep-crustal deformation.

Conrad discontinuity (Fig. 6c): The contoured surface of the Conrad discontinuity is constrained by seismic reflection and refraction data (grey lines in Fig. 6c). It has to be stressed, that the Conrad discontinuity is very poorly defined in the reflection seismic data (Figs 2a to 2d) and that the Conrad geometry might be more complex as appears in figure 6c. With this restriction in mind, the Conrad geometry strongly resembles the geometries of the underlying surfaces. The slightly smaller average dip angle (8°, as compared to 12° for the Moho and the laminated lower crust) implies a minor thickening of the lower crust towards the SSW. The same observation is made by YE (1992) in the EGT refraction profile. Comparison with the Conrad structure contour map of VALASEK (1992) reveals differences in depth and strike by a maximum of 2 km and 10°, respectively. These differences lie within the estimated error bounds. The lack of a reflective Conrad discontinuity towards the south (stippled contours in Fig. 6c) appears to be roughly coincident with the lack of a reflective laminated lower crust (compare Fig. 6b with 6c). We therefore propose the same explanation for the lack of the Conrad as for the lack of the reflective laminated lower crust (see above).

Top of crystalline basement (Fig. 6d): The structure contour map of the top of the crystalline basement shows the first basement unit encountered going downward from the topographic surface. The map is based on the 2D interpretations of the reflection data and on geological surface data (grey lines and surfaces in Fig. 6d).

The map's northwestern corner is characterized by an unstructured SSE-dipping surface. It strikes N66°E with a dip of 10°. This orientation is very similar to the orientation of the deep crustal discontinuities (Figs 6a to 6c) and is indicative of a relatively undisturbed European foreland crust. Immediately south of the autochthonous foreland, the basement-cover contact starts to rise to a maximum elevation of +1 km in the Vättis inlier to form the eastern Aar massif culmination (Fig. 1). The uplift shows the overall geometry of a dome, bordered by a depression in the N (marked by the northernmost basement thrust) and by the Gotthard thrust-sheet in the S. The northern flank of the dome which was seismically modelled by STÄUBLE and PFIFFNER (1991) and STÄUBLE et al. (1993) is characterized by overturned folds and thrust slices, whereas the southern side reveals a less complex geometry with a steep SSE-dip of approximately 50°. To the ENE, the basement uplift strongly diminishes in amplitude suggesting that the Aar massif culmination ceases to exist some kilometers further ENE.

To the S, the eastern Aar massif is shown to be overthrust by the S-Helvetic Gotthard thrust-

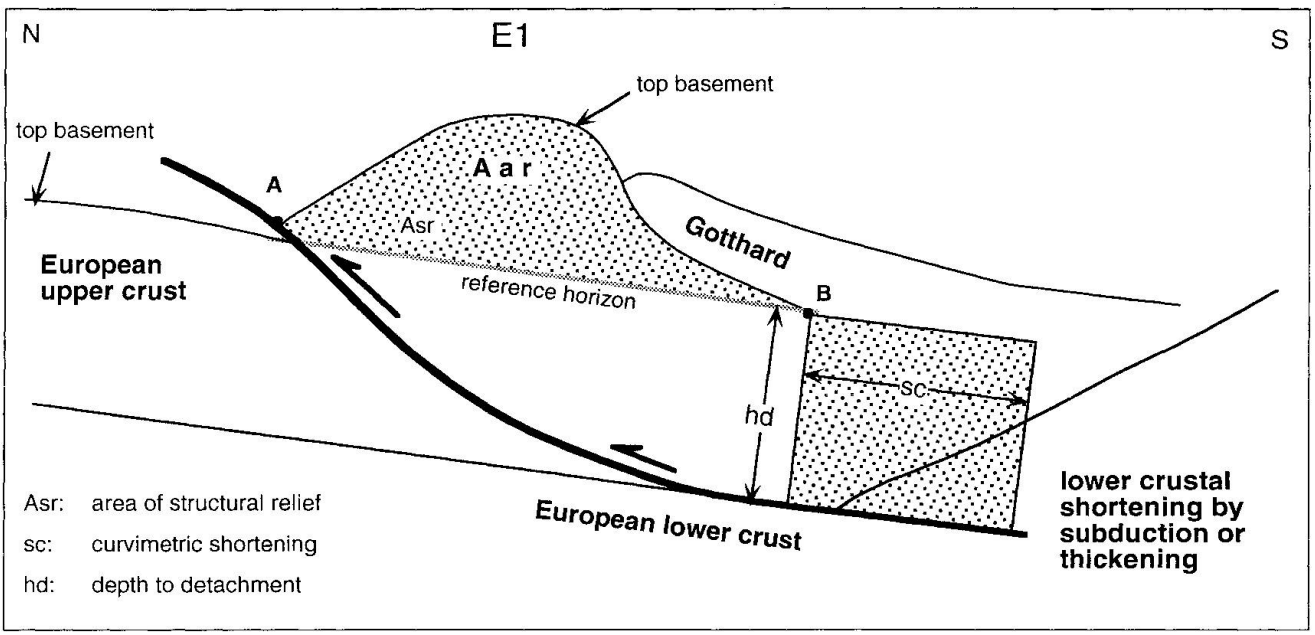

Fig. 7 Diagram illustrating depth-to-detachment calculation along line E1. The following estimates were obtained: area of structural relief A_{sr} = 350 km^2, curvimetric shortening s_c = 25 km, depth to detachment h_d = 14 km.

sheet. This second basement unit is considerably less constrained. Its overall geometry is that of a ENE dipping, slightly reclined antiform, lacking positive indications of internal fold-and-thrust structures such as observed in the Aar massif. In addition to this contrast in structural style, the eastern Gotthard "massif" seems to widen towards the WSW and ENE, indicating that it has been passively deformed by the uplift of the eastern Aar massif culmination.

To the S of the Gotthard thrust-sheet, the crystalline basement top is represented by the front of the N-Penninic Adula nappe. The latter's geometry is constrained by surface and reflection seismic data (see also LITAK et al., 1993). The frontal Adula nappe shows a change in geometry from an overturned ENE plunging antiform in the WSW to a more or less horizontal wedge-shaped body in the ENE. An average axial plunge of 20° can be deduced from the contours which is comparable to the axial plunge of the eastern Penninic nappe stack determined from surface data (e.g. MILNES and SCHMUTZ, 1978).

When comparing the top of the crystalline basement in figure 6d (based on seismic data) with the one in PFIFFNER et al. (1990a, based on surface data solely), significant differences emerge. For example, the top of the Aar massif N of the culmination is deeper by up to 3 km in the new map. Similarly, the top of the Gotthard thrust-sheet at coordinates 750/180 is at approximately –1.5 km in PFIFFNER et al. (1990a) but at –3.5 km in figure 6d. In addition, the top basement contour in the new map is more structured, illustrating that the cover sediments at the surface conceal important basement structures at depth.

Discussion and conclusion

The results of the deep seismic data presented here show, that the crust-mantle boundary, the top of the laminated lower crust and the Conrad discontinuity (Figs 6a to 6c) have similar 3D geometries with ENE strikes and dips between 12° (Moho, top laminated lower crust) and 8° (Conrad). The thickness of the laminated lower crust remains constant at around 4 to 5 km, whereas the thickness of the lower crust increases from 12 km in the N to 16 km in the S. This thickening is also reported from other NFP20 transects and the EGT refraction profile (VALASEK, 1992; YE, 1992). It indicates, that collision tectonics affected the European lower crust as far N as the external massifs.

In sharp contrast to the simple geometry of the lower crustal units, the top of the crystalline basement is structurally much more complex with reliefs of up to 10 km. The relief and the associated disharmony with the underlying units suggest that not only the nappes (Adula, etc.), but also the basement "massifs" (Aar, Gotthard) must be considered allochthonous. This implies that an intracrustal decoupling mechanism must have

taken place during the formation of the basement units. The decoupling horizon must be situated somewhere between the planar top of the lower crust and the deformed top of the crystalline basement. The depth to this detachment can be estimated using a combination of line length and area balancing (cf. LAUBSCHER, 1965; SUPPE, 1985) as briefly outlined below (Fig. 7). The rear end of the detached block is displaced by the distance s_c, which is the curvimetric shortening defined as:

$$s_c = l_o - l_c$$

where l_o is the original length, and l_c the current length of the displaced crustal block. These lengths are determined in the case of the Aar massif by measuring the length of the Triassic strata overlying the crystalline basement between points A and B (l_o) and the current length measured along the reference horizon (l_c). The reference horizon was chosen parallel to the lower crustal boundaries assuming a constant upper crustal thickness before detachment. Subtracting l_c from l_o the curvimetric shortening s_c can be estimated at 25 km for line E1. The area of structural relief, A_{sr}, corresponds to the area uplifted above the reference horizon. This area must be equal to the rectangle at the rear end of the displaced block (height = depth to detachment h_d, length = curvimetric shortening s_c). In the E1 transect A_{sr} for the Aar massif is about 350 km^2. From these figures the depth to detachment can be estimated at around 14 km. If one measures 14 km down from the top of the southern Aar massif in figure 5, the detachment is placed at approximately the level of the Conrad discontinuity. One arrives thus at the conclusion that at the time of deformation the basal detachment of the eastern external Aar massif was located near the top of the European lower crust.

The amount of upper crustal shortening in the external massifs has to be accommodated in the lower levels. Basically, two tectonic model endmembers for the coeval lower crustal shortening exist which are briefly outlined below. Model I (cf. PFIFFNER et al., 1990b) envisages a continental subduction in which the European lower crust is delaminated from the European upper crust and subducted southward under a northward indenting wedge of Adriatic lower crust. Model II (LAUBSCHER, 1994) sees the lower crustal shortening accommodated by stacking of lower crust imbrications with a decoupling at the base of the crust from the subducting mantle, i.e., no crustal material is subducted during the latest phase of Alpine shortening. A discussion of the two models is beyond the scope of this study. However, in the light of the low data quality concerning the lower crust in the internal domain, both models appear to be possible.

The highly structured basement-cover contact has its equivalent in the mapped pattern of the surface geology (Fig. 1). For example, the embayment of the basal Austroalpine thrust fault E of Vättis (with the sudden change in strike from N–S to SW–NE) can be clearly linked to the Aar massif culmination in the subsurface. Similarly, S of Vättis, the strike change from NE–SW to N–S of the Austroalpine base can be linked to the topography of the Gotthard and Adula units (note that this strike change at surface mimics the trend of the structure contours at subsurface). The basement topography is thus taken to be responsible for the general shape of the Prättigau halfwindow (as postulated, e.g., by STAUB, 1934), a fact which is also sustained by the orientation of the principal foliation plane in the Bündnerschiefer, dipping SSE in the area of Chur and E in the area of line E10 (Dreibündenstein phase of PFIFFNER, 1977).

Comparing the amplitude of the Aar massif's bulge in the N–S lines in figure 5 it is evident that the bulge (and thus the area of structural relief) decreases eastward from slightly over 10 km in line E1 to less than 4 km in line E9. The depth to detachment can only be estimated with some confidence in line E1 (where the Aar massif is exposed at the surface). In the case of, e.g., line E9 the structures allowing an assessment of the curvimetric shortening s_c are concealed completely by the overlying Penninic nappes. We tentatively explain the decrease in area of structural relief by a decrease in shortening, rather than a shallower basal detachment. The decrease in shortening associated with the eastern Aar massif can be thought of as being compensated by a transfer of shortening to the "Engadin uplift" located south and east of the Aar massif uplift. As discussed in HITZ and PFIFFNER (1995c), the ENE striking antiform associated with the Engadine window and which is outlined by the basal Austroalpine thrust, is cored by Penninic cover nappes. This antiform is locally uplifted in response to the thrusting of a NW-vergent upper crustal basement wedge resulting in the domal shape of the Engadine window. It seems possible, that this latter basement wedge is arranged in a right-step en-échelon manner in respect to the eastern external basement uplift. Similarly, as discussed in PFIFFNER et al. (1995), the western end of the Aar massif and the Aiguilles Rouges-Mt. Blanc massifs are relayed in a right-step en-échelon manner. Such a geometry is compatible to dextral transpression with NNW–SSE directed shortening between the European and Adriatic plates in Late

Tertiary times, as suggested by plate reconstructions by, e.g., SAVOSTIN et al. (1986).

Returning to the investigated area it can be concluded that:

1) The Moho discontinuity, the top of the laminated lower crust and the Conrad discontinuity have all similar and simple 3D geometries with a constant strike to the ENE and dip angles between 8° and 12°. The laminated lower crust has a constant thickness of 4 to 5 km, whereas the lower crust thickens from 12 km in the NNW to approximately 16 km in the SSE. This change in lower crustal thickness might reflect mild lower crustal thickening during Tertiary compression.

2) The 3D geometry of the structurally highest basement-cover contact reveals complicated domal surfaces predominantly formed by thrust tectonics. The structural disharmony with respect to the lower crust implies a crustal decoupling mechanism during the formation of the basement uplifts and nappes. The decoupling horizon must be situated between the Conrad discontinuity and the top of the crystalline basement.

3) Comparison of surface data and the top-basement geometry clearly reveals a kinematic link between the shape of the Prättigau halfwindow and the formation of the eastern Aar massif culmination.

Acknowledgements

We are indebted to J.-M. Marthelot for his critical review and helpful comments on this work and to J. Ansorge, G. Eisbacher and R. Marchant for reviewing an earlier version of the manuscript. L.H. likes to thank in particular J. Ansorge, H. Horstmeyer, E. Lanz and St. Mueller for help, many discussions and hospitality at the Institute of Geophysics ETHZ.

References

ALLEMANN, F., SCHWIZER, B., MARTIN, B. and HARTMANN, K. (1985): Geologische Karte des Fürstentums Liechtenstein 1 : 25'000. Regierung des Fürstentums Liechtenstein.

BOIS, C. and ECORS SCIENTIFIC PARTIES (1991): Post-orogenic evolution of the European crust studies from ECORS deep seismic profiles. In: Continental Lithosphere: Deep Seismic Reflections (Ed. by MEISSNER, R., BROWN, L., DÜRBAUM, H.J., FRANKE, W., FUCHS, K. and SEIFERT, F.), Amer. Geophys. Union, Geodynamics Series 22, 59–72.

BRAUCHLI, R. and LEUPOLD, W. (1915): Tektonische Karte des Plessurgebirges und der Ducankette. Vierteljahresschr. Naturf. Ges. Zürich 64.

BRAUCHLI, R. and GLASER, TH. (1924): Geologische Karte von Mittelbünden: Lenzerhorn. Sp.-K. Nr. 94C. Schweiz. Geol. Komm.

CADISCH, J. (1922): Geologische Karte von Mittelbünden. Blatt A: Arosa, Spezialkarte Nr. 94A. Schweiz. Geol. Komm.

CHRIST, P. and NABHOLZ, W. (1959): Geologische Generalkarte der Schweiz 1 : 200'000, Blatt 4, St. Gallen-Chur. Schweiz. Geol. Komm.

DEKORP (1990): DEKORP Atlas (ed. by MEISSNER, R. and BORTFELD, R.). Springer, Heidelberg.

EGLOFF, R. (1979): Sprengseismische Untersuchungen der Erdkruste in der Schweiz. Ph. D. Thesis, ETH Zürich, 167 pp.

EUGSTER, H. and LEUPOLD, W. (1930): Geologische Karte von Mittelbünden: Landwasser. Sp.-K. Nr. 94D. Schweiz. Geol. Komm.

FREI, W., HEITZMANN, P., LEHNER, P., MUELLER, ST., OLIVIER, R., PFIFFNER, O.A., STECK, A. and VALASEK, P. (1989): Geotraverses across the Swiss Alps. Nature 340, 544–548.

HITZ, L. and PFIFFNER, O.A. (1995a): Interpretation of line E2: The crustal structure along strike in the eastern Swiss Alps. In: Deep structure of Switzerland – Results from NFP20. Birkhäuser, Basel, in preparation.

HITZ, L. and PFIFFNER, O.A. (1995b): Interpretation of line E3: The deep structure of the Engadine window. In: Deep structure of Switzerland – Results from NFP20. Birkhäuser, Basel, in preparation.

HITZ, L. and PFIFFNER, O.A. (1995c): Deep seismic fan data and a 3D crustal model of the eastern Aar massif. In: Deep structure of Switzerland – Results from NFP20. Birkhäuser, Basel, in preparation.

HOLLIGER, K. and KISSLING, E. (1991): Ray theoretical depth migration: Methodology and application to deep seismic reflection data across the eastern and southern Swiss Alps. Eclogae geol. Helv. 84, 369–402.

HOLLIGER, K. and LEVANDER, A. (1994): Structure and seismic response of extended continental crust: Stochastic analysis of the Strona-Ceneri and Ivrea zones, Italy. Geology 22, 79–82.

KERN, H. and RICHTER, A. (1981): Temperature derivates of compressional and shear wave velocities in crustal and mantle rocks at 6 kbar confining pressure. J. Geophys. 49, 47–56.

LAUBSCHER, H.P. (1965): Ein kinematisches Modell der Jurafaltung. Eclogae geol. Helv. 58, 231–318.

LAUBSCHER, H.P. (1983): Detachment, shear, and compression in the Central Alps. Geol. Soc. Amer. Mem. 158, 191–211.

LAUBSCHER, H.P. (1994): Deep structure of the Central Alps in the light of recent seismic data. Geol. Rundsch. 83, 237–248.

LEVATO, L., SELLAMI, S., EPARD, J.L., PRUNIAUX, B., OLIVIER, R., WAGNER, J.L. and MASSON, H. (1994): The cover-basement contact beneath the Rawil axial depression (western Alps): true amplitude seismic processing, petrophysical properties, and modelling. Tectonophysics 232, 391–409.

LITAK, R.K., MARCHANT, R.H., PFIFFNER, O.A., BROWN, L.D., SELLAMI, S., LEVATO, L., WAGNER, J.-J. and OLIVIER, R. (1993): Crustal structure of the Swiss Alps from 3-D seismic modelling, Part II: Penninic nappes. Tectonics 12, 925–935.

LORENZ, TH. (1901): Geologische Karte des südlichen Rhätikon. Ber. Naturf. Ges. Freiburg i. Br. 12.

MILNES, A.G. and SCHMUTZ, H.U. (1978): Structure and History of the Suretta nappe (Pennine Zone, Central Alps) – a field study. Eclogae geol. Helv. 71, 19–33.

NABHOLZ, W.K. (1945): Geologie der Bündnerschiefergebirge zwischen Rheinwald, Valser- und Safiental. Eclogae geol. Helv. 38, 1–119.

NÄNNY, P. (1948): Zur Geologie der Prättigauschiefer zwischen Rhätikon und Plessur. Ph. D. Thesis, ETH Zürich, 128 pp.

OBERHAUSER, R. (1980): Molasse-Untergrund, Helvetikum, Flysche und Klippenzonen in Vorarlberg. In: Der geologische Aufbau Österreichs (ed. by OBERHAUSER, R.), 177–188, Springer, Wien.

PFIFFNER, O.A. (1977): Tektonische Untersuchungen im Infrahelvetikum der Ostschweiz. Ph. D. Thesis Nr. 5911, ETH Zürich, 432 pp.

PFIFFNER, O.A. (1985): Displacements along thrust faults. Eclogae geol. Helv. 78, 313–333.

PFIFFNER, O.A. (1993): The structure of the Helvetic nappes and its relation to the mechanical stratigraphy. J. Struct. geol. 15, 511–521.

PFIFFNER, O.A., KLAPER, E.M., MAYERAT, A.M. and HEITZMANN, P. (1990a): Structure of the basement-cover contact in the Swiss Alps. In: Deep structure of the Alps (ed. by ROURE, F., HEITZMANN, P. and POLINO, R.), Mém. Soc. géol. France 156, 247–262.

PFIFFNER, O.A., FREI, W., VALASEK, P., STÄUBLE, M., LEVATO, L., DUBOIS, L., SCHMID, S.M. and SMITHSON, S.B. (1990b): Crustal shortening in the Alpine orogen: Results from deep-seismic reflection profiling in the Eastern Swiss Alps, line NFP20-EAST. Tectonics 9, 1327–1355.

PFIFFNER, O.A. and HITZ, L. (1995): Seismic line E1: Crustal shortening in the transect trough the Helvetic and Penninic nappes and the Adriatic indenter. In: Deep structure of Switzerland – Results from NFP20. Birkhäuser, Basel, in preparation.

PFIFFNER, O.A., SAHLI, S. and STÄUBLE, M. (1995): Structure and evolution of the external basement massifs (Aar, Aiguilles Rouges / Mt. Blanc). In: Deep structure of Switzerland – Results from NFP20. Birkhäuser, Basel, in preparation.

REY, P. (1993): Seismic and tectono-metamorphic characters of the lower continental crust in Phanerozoic areas: a consequence of post-thickening extension. Tectonics 12, 580–590.

SAVOSTIN, L.A., SIBUET, J.-C., ZONENSCHAIN, L.P., LE PICHON, X. and ROULET, M.-J. (1986): Kinematic Evolution of the Tethys Belt from the Atlantic Ocean to the Pamirs since the Triassic. Tectonophysics 123, 1–35.

SPRECHER, C. and MÜLLER, W.H. (1986): Geophysikalisches Untersuchungsprogramm Nordschweiz: Reflexionsseismische Messungen 82. Nagra Tech. Ber. (NTB) 84-15, 168 pp.

STAUB, R. (1934): Grundzüge und Probleme alpiner Morphologie. Denkschr. Schweiz. Naturf. Ges. 69.

STÄUBLE, M. and PFIFFNER, O.A. (1991): Evaluation of the seismic response of basement fold-and-thrust geometry in the Central Alps based on 2-D ray tracing. Annales Tectonicae 5, 3–17.

STÄUBLE, M., PFIFFNER, O.A. and SMITHSON, S.B. (1993): Crustal structure and reflectivity of the Swiss Alps from 3-D Seismic Modelling, Part I: Helvetic nappes. Tectonics 12, 911–924.

SUPPE, J. (1985): Principles of Structural Geology. Prentice Hall, Englewood Cliffs, 537 pp.

TOLLMANN, A. (1976): Der Bau der Nördlichen Kalkalpen. Franz Deuticke, Wien, 449 pp.

TRÜMPY, D. (1916): Geologische Karte des Falknis. Spezialkarte Nr. 79. Schweiz. Geol. Komm.

TRÜMPY, R. (1969): Die helvetischen Decken der Ostschweiz. Versuch einer palinspastischen Korrelation und Ansätze zu einer kinematischen Analyse. Eclogae geol. Helv. 62, 105–142.

TRÜMPY, R. (1980): Geology of Switzerland – a guide book. Part A: An outline of the geology of Switzerland. Wepf and Co., Basel, 104 pp.

TRÜMPY, R. (1992): Ostalpen und Westalpen – Verbindendes und Trennendes. Jb. Geol. B.-A. 135, 875–882.

VALASEK, P. (1992): The tectonic evolution of the Swiss Alpine crust interpreted from a 2D network of deep crustal seismic profiles and an evaluation of 3D effects. Ph.D. Thesis Nr. 9637, ETH Zürich, 196 pp. with annex 142 pp.

VALASEK, P., MUELLER, St., FREI, W. and HOLLIGER, K. (1991): Results of NFP20 seismic reflection profiling along the Alpine section of the European Geotraverse (EGT). Geophys. J. Int. 105, 85–102.

WYSS, R. (1986): Die Urseren-Zone – Lithostratigraphie und Tektonik. Eclogae geol. Helv. 79, 73–767.

YAN, Q.Z. and MECHIE, J. (1989): A fine structural section through the crust and lower lithosphere along the axial region of the Alps. Geophys. J. 98, 465–488.

YE, S. (1992): Crustal structure beneath the Central Swiss Alps derived from seismic refraction data. Ph. D. Thesis Nr. 9631, ETH Zürich, 122 pp.

Manuscript received August 2, 1994; minor revision accepted October 1, 1994.